Journal of Hazardous Materials 195 (2011) 346–354

Contents lists available at SciVerse ScienceDirect

Journal of Hazardous Materials

journal homepage: www.elsevier.com/locate/jhazmat

Rose-like monodisperse bismuth subcarbonate hierarchical hollow microspheres: One-pot template-free fabrication and excellent visible light photocatalytic activity and photochemical stability for NO removal in indoor air

Fan Dong[a,b,c], S.C. Lee[b,*], Zhongbiao Wu[c], Yu Huang[b], Min Fu[a], Wing-Kei Ho[d], Shichun Zou[e], Bo Wang[b]

[a] College of Environmental and Biological Engineering, Chongqing Technology and Business University, Chongqing, 400067, PR China
[b] Department of Civil and Structural Engineering, Research Center for Environmental Technology and Management, The Hong Kong Polytechnic University, Hong Kong, PR China
[c] Department of Environmental Engineering, Zhejiang University, Hangzhou 310027, PR China
[d] Nano and Advanced Materials Institute Limited, Hosted by The Hong Kong University of Science and Technology, Hong Kong, PR China
[e] School of Marine Sciences, Sun Yat-Sen University, Guangzhou, 510275, PR China

ARTICLE INFO

Article history:
Received 29 May 2011
Received in revised form 5 August 2011
Accepted 16 August 2011
Available online 22 August 2011

Keywords:
$(BiO)_2CO_3$
Hollow microsphere
Visible light
Photocatalytic
Indoor air

ABSTRACT

Rose-like monodisperse hierarchical $(BiO)_2CO_3$ hollow microspheres are fabricated by a one-pot template-free method for the first time based on hydrothermal treatment of ammonia bismuth citrate and urea in water. The microstructure and band structure of the as-prepared $(BiO)_2CO_3$ superstructure are characterized in detail by X-ray diffraction, Raman spectroscopy, Fourier transform-infrared spectroscopy, transmission electron microscopy, scanning electron microscopy, N_2 adsorption–desorption isotherms, X-ray photoelectron spectroscopy and UV–vis diffuse reflectance spectroscopy. The monodisperse hierarchical $(BiO)_2CO_3$ microspheres are constructed by the self-assembly of single-crystalline nanosheets. The aggregation of nanosheets result in the formation of three dimensional hierarchical framework containing mesopores and macropores, which is favorable for efficient transport of reaction molecules and harvesting of photo-energy. The result reveals the existence of special two-band-gap structure (3.25 and 2.0 eV) for $(BiO)_2CO_3$. The band gap of 3.25 eV is intrinsic and the formation of smaller band gap of 2.0 eV can be ascribed to the in situ doped nitrogen in lattice. The performance of hierarchical $(BiO)_2CO_3$ microspheres as efficient photocatalyst are further demonstrated in the removal of NO in indoor air under both visible light and UV irradiation. It is found that the hierarchical $(BiO)_2CO_3$ microspheres not only exhibit excellent photocatalytic activity but also high photochemical stability during long term photocatalytic reaction. The special microstructure, the high charge separation efficiency due to the inductive effect, and two-band-gap structure in all contribute to the outstanding photocatalytic activities. The discovery of monodisperse hierarchical nitrogen doped $(BiO)_2CO_3$ hollow structure is significant because of its potential applications in environmental pollution control, solar energy conversion, catalysis and other related areas.

1. Introduction

Many materials in the nature, such as lotus leaf and seashell, consisting of ordinary composition, exhibit fascinating properties owing to their special structural characteristics [1,2]. Such intricate natural designs have inspired materials scientists to fabricate morphology and structure controlled materials, with expectations to obtain novel or enhanced properties [2–4].

Hierarchical hollow structured materials have been a subject of intensive research in the past decade because of their novel physicochemical properties, which differ markedly from those of bulk materials, and their potential applications as nanoscale chemical reactors, (photo)catalysts, sensing, lithium batteries, solar energy conversion, photonic building blocks and environmental applications, to name a few [5–10]. The fabrication of such structures usually relies on templating approaches, in which hard templates [11–14] (e.g., monodisperse polymer latex, carbon, silica spheres, and reducing metal nanoparticles) or soft sacrificial templates [15–19] (e.g., micelles, microemulsions, macromolecules, oil droplets, and gas bubbles) were used to direct the growth of hierarchical or hollow structure.

The template approach can be easily conducted for a specific structure. The capability of constructing complicated structure, however, is usually limited by the availability of templates. Disadvantages related to high cost and tedious synthetic procedures have also impeded scale-up of these template methods for

* Corresponding author. Tel.: +852 27666011; fax: +852 27666011.
E-mail address: ceslee@polyu.edu.hk (S.C. Lee).

0304-3894/$ – see front matter © 2011 Elsevier B.V. All rights reserved.
doi:10.1016/j.jhazmat.2011.08.050

applications. In comparison with these methods, which involve multistep procedures, a one-pot template-free approach for the controlled synthesis of hierarchical hollow sphere is highly attractive and desirable based on different mechanisms. Recently, a number of one-pot template-free methods for generating hollow inorganic micro- and nanostructures have been developed by using some well-known physical phenomena, for example, Ostwald-ripening [20], Kirkendall-effect [21] and oriented attachment [22].

Recently, there has been great interest in developing semiconductor photocatalysts with high activities (especially the visible light driven photocatalysts) for both energetic and environmental applications, such as photocatalytic hydrogen evolution, creation of self-cleaning surfaces, disinfection of water, degradation of organic contaminants and conversion of carbon dioxide into hydrocarbon fuels [23–32]. The key to the application of photocatalysis technology is to develop photocatalytic materials with efficient activity and high stability. Photocatalytic materials with hollow or hierarchical structure, such as TiO_2 [33,34], ZnS [35], WO_3 [36], $BiVO_4$ [37], Bi_2WO_6 [38] and Cu_2PO_4OH [39] have been fabricated by different methods, and are proved to be high-performance in environmental pollutants degradation due to their special morphological structure with respect to pore structure, light harvesting, and charge separation and so on. Development of new visible light driven photocatalytic materials may also overcome the limitations of transitional TiO_2 (reduced sensitivity to sunlight and limited visible light photocatalytic activity) [25]. Controlling the shape and morphology of new photocatalytic materials may, therefore provide new opportunities to explore their novel structural properties and photocatalytic activity. In spite of these advances, realization of controlled one-pot fabrication of novel hierarchical hollow structure by facile template-free method remains a great challenge.

The bismuth subcarbonate $(BiO)_2CO_3$ is first reported in 1984 [40]. It has an orthorhombic crystal structure with cell parameters of $a = 3.865$, $b = 3.865$, and $c = 13.675$ Å, belonging to *Imm2* space group. After the first report in 1984, there is little investigation on the fabrication and properties of $(BiO)_2CO_3$. Until very recently, synthetic $(BiO)_2CO_3$ is reported to display promising results in antibacterial and environmental applications [41–43]. Although some advances has been made, much is unknown on the controlled fabrication, morphological structure, especially the visible light photocatalytic properties of uniform hierarchical $(BiO)_2CO_3$ hollow microspheres. It will be, therefore of fundamental and technological interest to develop facile and effective methods for the fabrication of such novel structured $(BiO)_2CO_3$ with novel properties for energetic and environmental applications [28].

In this study, we developed a one-pot template-free method for the fabrication of uniform monodisperse hierarchical $(BiO)_2CO_3$ hollow microspheres for the first time based on hydrothermal reaction between ammonia bismuth citrate and urea. The as-prepared hierarchical $(BiO)_2CO_3$ microspheres were analyzed by various characterization tools to fully understand the structural properties and were used as visible light photocatalyst for indoor air NO removal. It was found that the attractive hierarchical $(BiO)_2CO_3$ microspheres were constructed by self-assembly of single-crystalline nanosheets. Interestingly, nitrogen was in situ doped into the lattice of $(BiO)_2CO_3$, which modified the band structure significantly. For the first time, the monodisperse hierarchical $(BiO)_2CO_3$ hollow microspheres were found to exhibit excellent photocatalytic activity and photochemical stability for indoor air NO removal under both visible and UV light irradiation. The attractive hierarchical $(BiO)_2CO_3$ hollow microspheres will also find wide application in other areas, such as solar energy conversion, aqueous pollution control and production of fuels by fully using solar energy.

2. Experimental

2.1. Fabrication

All chemicals used in this study were analytical grade (Sigma–Aldrich) and were used without further purification. Distilled water was used in all experiments. In a typical synthesis, appropriate amounts of ammonia bismuth citrate (1.66 g) and urea (0.72 g) were mixed with 75 ml of H_2O in a 100 ml autoclave Teflon vessel and stirred for 30 min. The resulted transparent precursor solution was then hydrothermally treated at 180 °C for 12 h. The sample obtained was filtered, washed with water and ethanol for four times and dried at 60 °C to get final $(BiO)_2CO_3$ with no further treatment. For comparison, C-doped TiO_2 were prepared by reported hydrothermal method [29] and the commercial Degussa P25 was also used as reference sample.

2.2. Characterization

The crystal phases of the sample were analyzed by X-ray diffraction with Cu Kα radiation (XRD: model D/max RA, Rigaku Co., Japan). The accelerating voltage and the applied current were 40 kV and 150 mA, respectively. Raman spectra were recorded at room temperature using a micro-Raman spectrometer (Raman: RAMANLOG 6, USA) with a 514.5 nm Ar + laser as the excitation source in a backscattering geometry. The incident laser power on the samples was less than 10 mW. X-ray photoelectron spectroscopy with Al Kα X-rays ($h\nu = 1486.6$ eV) radiation operated at 150 W (XPS: Thermo ESCALAB 250, USA) was used to investigate the surface properties and to probe the total density of the state (DOS) distribution in the valence band (VB). The shift of the binding energy due to relative surface charging was corrected using the C1s level at 284.8 eV as an internal standard. FT-IR spectra were recorded on a Nicolet Nexus spectrometer on samples embedded in KBr pellets. A scanning electron microscope (SEM, JEOL model JSM-6490, Japan) was used to characterize the morphology of the obtained products. The morphology, structure and grain size of the samples were examined by transmission electron microscopy (TEM: JEM-2010, Japan). The UV–vis diffuse reflection spectra were obtained for the dry-pressed disk samples using a Scan UV–vis spectrophotometer (UV–vis DRS: TU-1901, China) equipped with an integrating sphere assembly, using $BaSO_4$ as reflectance sample. The spectra were recorded at room temperature in air ranged from 250 to 800 nm. Nitrogen adsorption–desorption isotherms were obtained on a nitrogen adsorption apparatus (ASAP 2020, USA). All the samples were degassed at 200 °C prior to measurements.

2.3. Photocatalytic activity evaluation

The photocatalytic activity of the resulting samples was investigated by oxidation of NO at ppb levels in a continuous flow reactor at ambient temperature. The volume of the rectangular reactor, which was made of stainless steel and covered with Saint-Glass, was 4.5 L (30 cm × 15 cm × 10 cm). A 300 W commercial tungsten halogen lamp (General Electric) was vertically placed outside the reactor above the reactor. Four mini-fans were fixed around the lamp to avoid the temperature rise of the flow system. Adequate distance was also kept from the lamp to the reactor for the same purpose to keep the temperature at a constant level. The distance between the lamp and the sample is 30 cm. For the visible light photocatalytic activity test, UV cutoff filter (420 nm) was adopted to remove UV light in the light beam. For photocatalytic activity test under simulated solar light, the UV cutoff filter was removed. For UV light photocatalytic activity test, two 6 W UV lamps (Cole–Parmler), emitting a primary wavelength at 365 nm was used. For each photocatalytic activity test experiment, one

sample dish (with a diameter of 12 cm) containing the photocatalyst powders was placed in the center of the reactor. The photocatalyst samples were prepared by coating an aqueous suspension of the samples onto the glass dish. The weight of the photocatalysts used for each experiment was kept at 0.15 g. The dishes containing the photocatalyst were pretreated at 70 °C for several hours until complete removal of water in the suspension and then cooled to room temperature before the photocatalytic test. The NO gas was acquired from a compressed gas cylinder at a concentration of 100 ppm of NO (N_2 balance, BOC gas) with traceable National Institute of Standards and Technology (NIST) standard. The initial concentration of NO was diluted to about 400 ppb by the air stream supplied by a zero air generator (Thermo Environmental Inc., model 111). The desired relative humidity (RH) level of the NO flow was controlled at 70% by passing the zero air streams through a humidification chamber. The gas streams were premixed completely by a gas blender, and the flow rate was controlled at 3.3 L/min by a mass flow controller. After the adsorption–desorption equilibrium among water vapor, gases, and photocatalysts was achieved, the lamp was turned on. The concentration of NO was continuously measured by a chemiluminescence NO analyzer (Thermo Environmental Instruments Inc., model 42c), which monitors NO, NO_2, and NO_x (NO_x represents $NO + NO_2$) with a sampling rate of 0.7 L/min. The removal efficiency (η) of NO was calculated as $\eta\,(\%) = (1 - C/C_0) \times 100\%$, where C and C_0 are concentrations of NO in the outlet steam and the feeding stream, respectively.

3. Results and discussion

3.1. Crystal phase

Fig. 1 shows the XRD pattern of the as-prepared hierarchical $(BiO)_2CO_3$ hollow microspheres compared with standard PDF card (JCPDS-ICDD Card No. 41-1488). All the diffraction peaks can be indexed to $(BiO)_2CO_3$. No peaks from other phases have been detected, indicating the phase purity of the product. The crystal structure of $(BiO)_2CO_3$ is shown in Fig. S1 (supporting information). The $(Bi_2O_2)^{2+}$ layers and CO_3^{2-} layers are inter-grown with the plane of the CO_3^{2-} group orthogonal to the plane of the $(Bi_2O_2)^{2+}$ layer. The large cation Bi^{3+} with 8-coordination shows stereo active lone-pair behaviors that results in the Bi–O polyhedron. The internal layered structure would guide the lower growth rate along certain axis to form nanosheet morphologies [44].

3.2. Vibrational spectra

The vibrational spectra of FT-IR and Raman obtained are shown in Fig. 2. The "free" carbonate ion (point group symmetry D_{3h}) possessed four internal vibrations: symmetric stretching mode ν_1, the corresponding antisymmetric vibration ν_3, the out-of-plane bending mode ν_2 and the in-plane deformation ν_4. Four characteristic bands in FT-IR at ν_1 (1067 cm^{-1}), ν_2 (846 and 820 cm^{-1}), ν_3 (1468 and 1391 cm^{-1}), ν_4 (670 cm^{-1}), $\nu_1 + \nu_4$ (1756 and 1730 cm^{-1}) are observed (Fig. 2a). The Raman bands at 1070, 1407 and 690 cm^{-1} are attributed to ν_1, ν_3 and ν_4 of the carbonate ion CO_3^{2-} vibration, respectively (Fig. 2b). The ν_2 mode is absent in the Raman spectra, indicating ν_2 is only IR active. The Raman band at 512 cm^{-1} can be assigned to the Bi=O stretching. The low bands at 417 and 162 cm^{-1} in Raman are due to the external vibration, which were also observed in other reports [45].

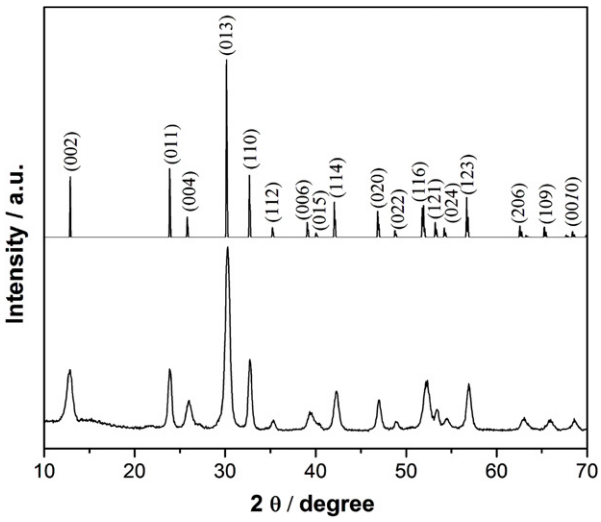

Fig. 1. XRD pattern of the as-prepared hierarchical $(BiO)_2CO_3$ microspheres.

3.3. Morphological structure

The hydrothermal treatment of ammonia bismuth citrate and urea mixture produces a population of hierarchical microspheres with an interesting rose-like shape, each containing a concavity on its center, as shown in the typical SEM images in Fig. 3. The as-prepared $(BiO)_2CO_3$ microspheres have an average diameter of 1.0 μm and thickness of 0.5 μm. No other morphologies can be observed, indicating a high yield of such $(BiO)_2CO_3$ superstructure. All the microspheres in Fig. 3a and b show almost the same size and are separated to each other, indicating the produced microspheres are highly uniform and monodisperse. The higher magnification SEM image shown in Fig. 3c reveals that each microsphere is

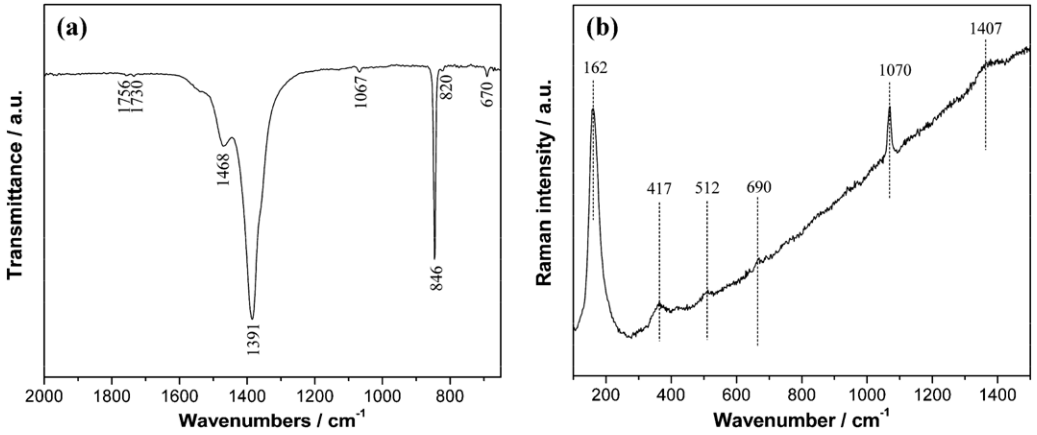

Fig. 2. FT-IR (a) and Raman (b) spectra of the as-prepared hierarchical $(BiO)_2CO_3$ microspheres.

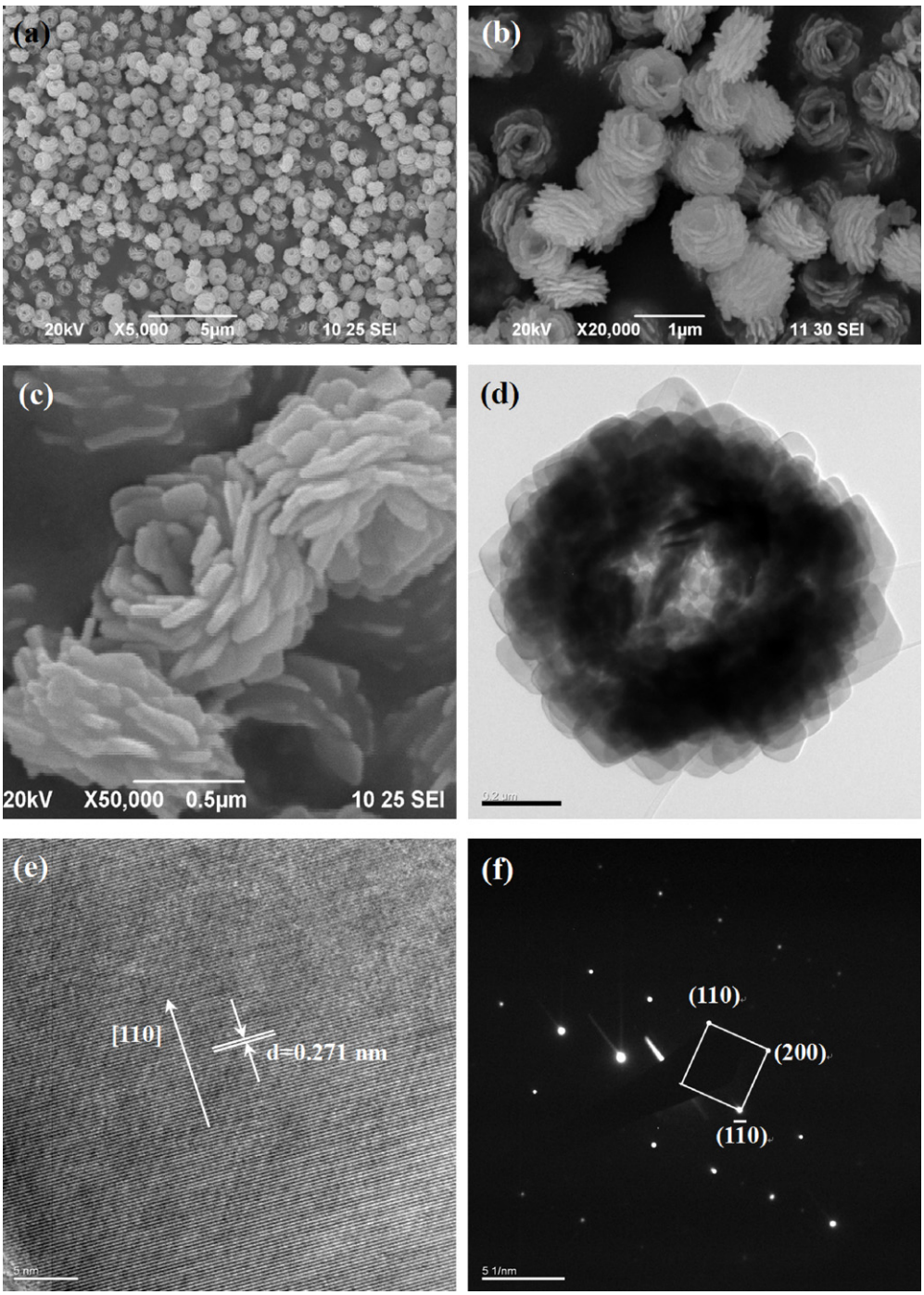

Fig. 3. SEM (a–c), TEM (d, e) the as-prepared hierarchical $(BiO)_2CO_3$ microspheres, SAED (f) of a single nanosheet.

composed of many layers of nanoscale sheet-like structures. These nanosheets are arranged at progressively increasing angles to the radial axis and are highly directed to form arrays in a hierarchical fashion. The side view of an individual rose-like structure (Fig. 3c) supports the conclusion that such a microsphere is composed of regularly packed nanosheets with an average thickness of about 20 nm.

The morphology and size of the product was further investigated by TEM. As shown in Fig. 3d, the entire microsphere is composed of self-assembled nanosheets. The nanosheets are very thin and therefore relatively transparent to the electron beam. The microsphere is hollow in the center. An HRTEM image of a single nanosheet in the microsphere is shown in Fig. 3e. The lattice spacing is measured to be 0.271 nm, matching with the spacing of the (1 1 0) crystal plane of $Bi_2O_2CO_3$. The SAED pattern in Fig. 3f displays an array of clear and regular diffraction spots of one single nanosheet, indicating that the nanosheet is well-defined single-crystalline in nature. Thus, the hierarchical $Bi_2O_2CO_3$ microspheres originates from the self-assembly of the single-crystalline nanosheets with preferred orientation.

In this fabrication approach, $(BiO)_2CO_3$ with particle morphology would be produced when urea was replaced by the same molar amount of sodium carbonate (see Fig. S2 and S3 in the supporting information). That is, the addition of urea plays a crucial role in forming hierarchical microsphere structure. It is known that urea can be decomposed in aqueous solution at an elevated temperature.

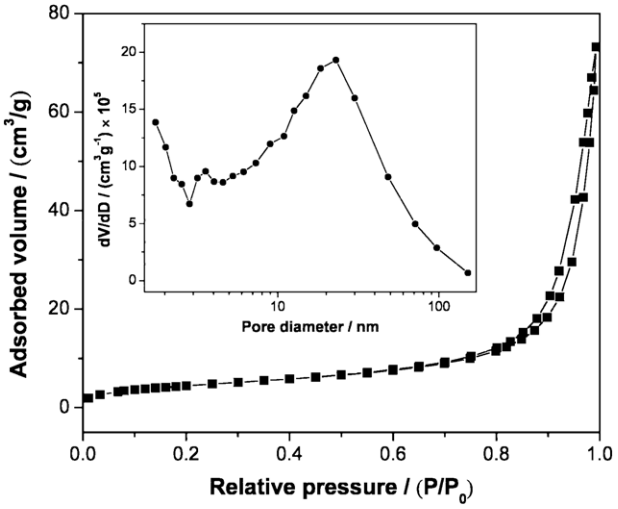

Fig. 4. N_2 adsorption–desorption isotherms and pore-size distribution (inset) of hierarchical $(BiO)_2CO_3$ microspheres.

The following reaction may take place in the hydrothermal process.

$$CO(NH_2)_2 + H_2O \rightarrow CO_2 + 2NH_3 \quad (1)$$

$$NH_3 + H_2O \rightarrow NH_4^+ + OH^- \quad (2)$$

$$CO_2 + 2OH^- \rightarrow CO_3^{2-} + H_2O \quad (3)$$

$$Bi^{3+}(\text{citrate}) + H_2O \rightarrow BiO^+ + 2H^+ \quad (4)$$

$$2BiO^+ + CO_3^{2-} \rightarrow (BiO)_2CO_3(s) \quad (5)$$

It is worthwhile and interesting to elucidate the growth mechanism of hierarchical $(BiO)_2CO_3$ hollow microspheres. As the growth mechanism is complicated, the precise understanding is in currently progress.

3.4. BET surface areas and pore structure

Fig. 4 shows nitrogen adsorption–desorption isotherms and the corresponding pore-size distribution (PSD) curves (inset in Fig. 4) for the as-prepared hierarchical $(BiO)_2CO_3$ microspheres. Nitrogen adsorption–desorption isotherm show hysteresis loops at relative pressures close to unity, indicating the presence of large mesopores (about 23.0 nm), which categorize it as type IV according to IUPAC classification [46]. The shape of adsorption branch at relative pressures is close to unity resemblances somewhat type II, indicating the presence of macropores [46]. The shapes of hysteresis loops are of type H3, associated with mesopores present in hierarchical nanosheet particles, giving rise to slit-like pores, which is consistent with the TEM results (Fig. 3). The isotherm also shows high adsorption at relative pressures (P/P_0) approaching 1.0, suggesting the formation of large mesopores and macropores [46]. In fact, the mesopores and macropores are formed due to aggregation of nanosheets, because the single-crystal nanosheets do not contain mesopores and macropores. As can be seen from this inset the PSD curve is quite broad (from 2 to 100 nm) and bimodal with small mesopores (~3.6 nm) and larger ones (~23.0 nm). The smaller mesopores reflect porosity within nanosheets, while larger mesopores can be related to the pores formed between stacked nanosheets. This result further confirmed the existence of mesopores and macropores. Such organized porous structures might be extremely useful in photocatalysis because they possess efficient transport pathways to reactant and product molecules [33,47]. The unique three dimensional macroporous hierarchical framework is also well suited for harvesting photo-energy and introducing reactive molecules into the interior space of hierarchical $(BiO)_2CO_3$ microspheres [48].

3.5. XPS analysis

The XPS measurements were carried out to determine the chemical state of the elements and total density of states distribution (DOS) of the valence band in as-prepared $(BiO)_2CO_3$, as shown in Fig. 5. Two strong peaks at 159.2 and 164.5 eV in the high-resolution spectra (Fig. 5a) are assigned to $Bi_4f_{7/2}$ and $Bi_4f_{5/2}$, respectively, which is characteristic of Bi^{3+} in $(BiO)_2CO_3$ [49]. Fig. 5b shows the C1s spectra of $(BiO)_2CO_3$. A broad energy range from 291 to 282 eV can be observed. The peaks at 284.8, 286.2 and 288.0 eV can be assigned to adventitious carbon species from XPS measurement [29], while the peak at 289.0 eV can be ascribed to carbonate ion in $(BiO)_2CO_3$. Meanwhile, the O1s spectra are also recorded (Fig. 5c), which can be fitted by three peaks at binding energies of 530.3, 531.3 and 532.4 eV, respectively. The peak at 530.3 eV is characteristic of Bi–O binding energy in $(BiO)_2CO_3$ [49], and the other two peaks at around 531.3 and 532.4 eV can be assigned to carbonate species and adsorbed H_2O on the surface. Nitrogen is detected by XPS with N1s binding energy centered at 400 eV as shown in Fig. 5d. This fact indicates that nitrogen was in situ doped into the $(BiO)_2CO_3$ during hydrothermal treatment. The N1s peak at 400 eV was also observed in the widely investigated nitrogen doped TiO_2, where nitrogen substituted for oxygen in TiO_2 [50–52]. In our case, nitrogen may also be doped into the lattice of $(BiO)_2CO_3$ and substitute for oxygen atom. The DOS of VB is shown in Fig. 5e. The valence band maximum (VBM) is determined to be 1.7 eV. Interestingly, additional diffusive electronic states above the VBM are observed above the valence band edge, indicating the existence of mid-gap above the valence band [53,54]. Such mid-gap can be ascribed to the nitrogen doping, similar to that of nitrogen doped TiO_2 [53,54]. The newly formed mid-gap between valence band and conduction band could make $(BiO)_2CO_3$ microspheres absorb visible light.

3.6. UV–vis DRS and band structure

The as-prepared hierarchical $(BiO)_2CO_3$ microspheres show a light yellow color, suggesting their ability to absorb light in the visible region. The UV–vis DRS of the materials in Fig. 6a shows two band-edge absorptions, one at UV region and another at visible light region. The $(BiO)_2CO_3$ can, thus absorb both UV and visible light. The band gap energy can be estimated from the intercept of the tangents to the plots of $(\alpha h\nu)^{1/2}$ vs. photon energy, as shown in Fig. 6b. Very interesting, the as-prepared $(BiO)_2CO_3$ shows two band gaps of 3.25 and 2.0 eV, consistent with additional diffusive electronic states observed with VB-XPS [25]. Khan et al. also observed the two-band-gap structure (3.0 and 2.32 eV) for carbon doped TiO_2, where the band gap of 3.0 eV was intrinsic for TiO_2 and the smaller band gap of 2.0 eV caused by the doped carbon in lattice [55]. In our case, the band gap of 3.25 eV is intrinsic for $(BiO)_2CO_3$, similar to report by Xie and Huang [42,43]. The smaller band gap of 2.0 eV can be due to the in situ doped nitrogen in lattice forming mid-gap. The as-prepared $(BiO)_2CO_3$ is, therefore sensitive to both UV and visible light.

It is noteworthy that CO_3^{2-} ions having a large negative charge, maintains a large dipole in the $(BiO)_2CO_3$, which prefers the photogenerated charge separation [56]. This effect is called an inductive effect, which can be described as the action of one group to affect the electron distribution in another group though electrostatic force [56]. The inductive effect prefers to attract holes and repel electrons, thus enhancing the photogenerated charge separation. It is thus expected that the hierarchical $(BiO)_2CO_3$ microspheres may exhibit high photocatalytic activity under both visible and UV light

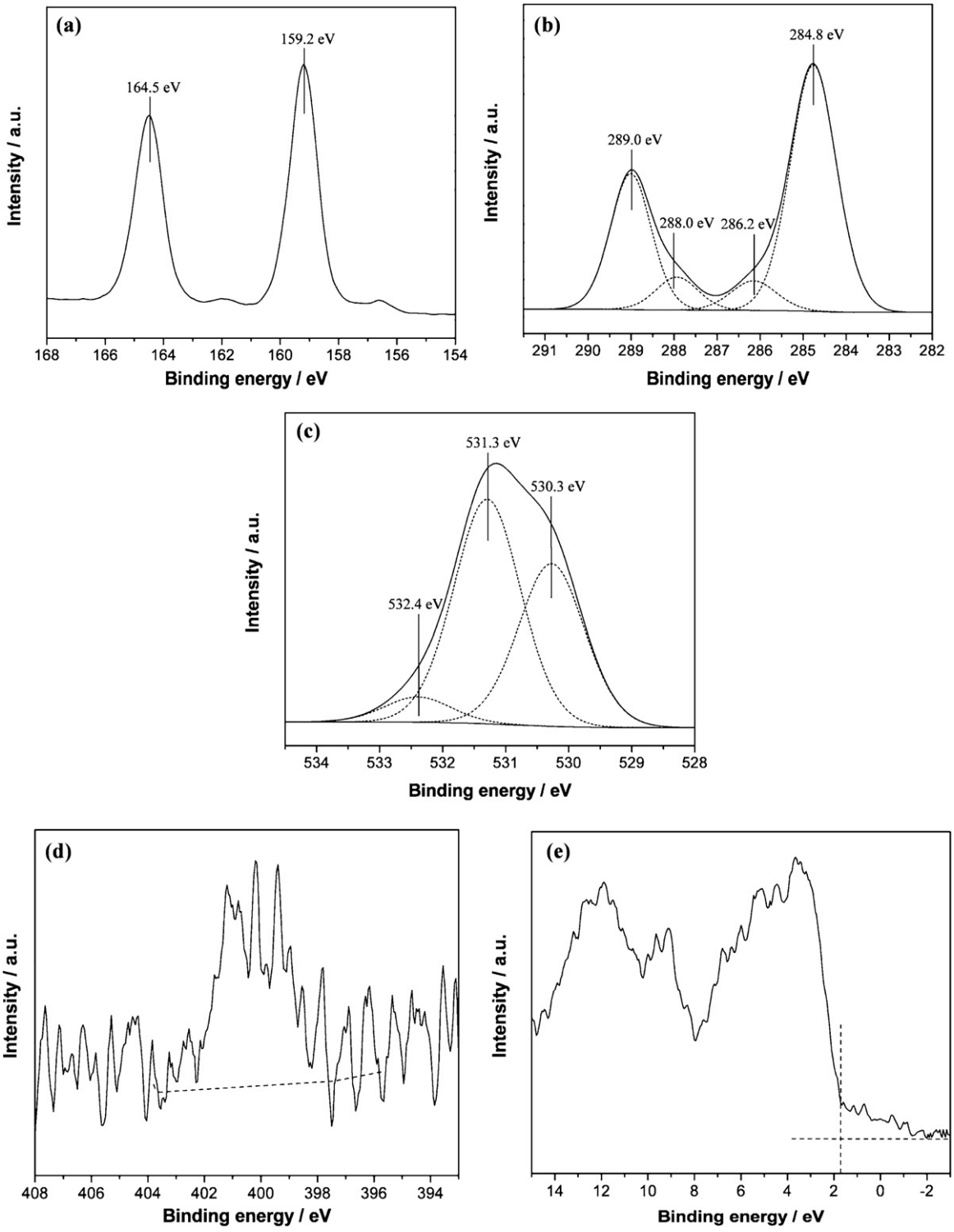

Fig. 5. XPS spectra of the as-prepared hierarchical $(BiO)_2CO_3$, (a) Bi_4f, (b) C1s, (c) O1s, (d) N1s and (e) VB.

irradiation, fully using solar light for degradation of environmental pollutants.

3.7. Photocatalytic activity and photochemical stability

3.7.1. Photocatalytic activities under visible and UV light irradiation

The as-prepared hierarchical $(BiO)_2CO_3$ microspheres were used to photocatalytic removal of NO in gas phase in order to demonstrate their potential ability for indoor air purification (Fig. 7). Fig. 7a shows the variation of NO concentration (C/C_0%) with irradiation time over the hierarchical $(BiO)_2CO_3$ microspheres under visible light irradiation. Here, C_0 is the initial concentration of NO, and C is the concentration of NO after photocatalytic reaction for t. As a comparison, photocatalytic oxidation of NO over C-doped TiO_2 and $(BiO)_2CO_3$ particles are also performed under identical conditions. As previously proved, NO could not be photolyzed under light irradiation ($\lambda > 420$ nm) [57]. As shown in Fig. 7a, after

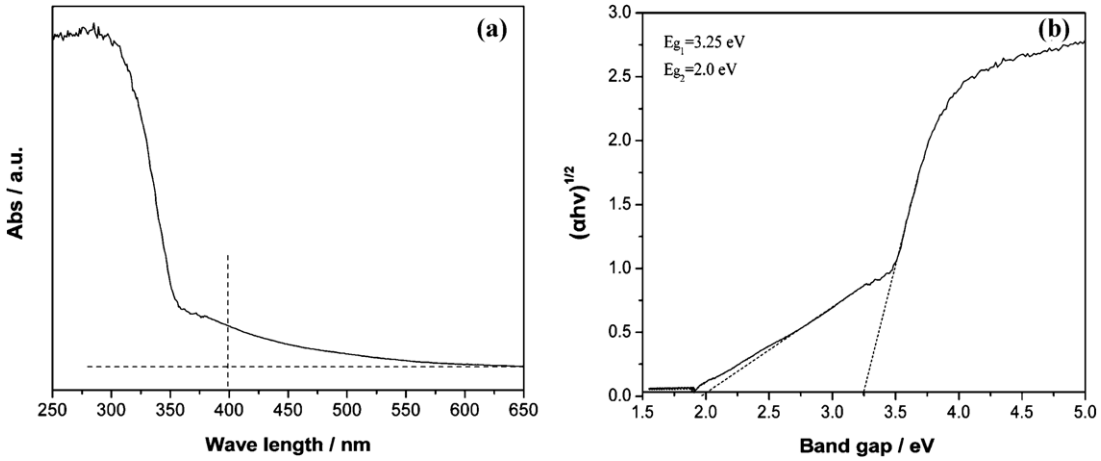

Fig. 6. UV–vis DRS (a) and plots of $(\alpha h\nu)^{1/2}$ vs. photon energy (b) of the as-prepared hierarchical $(BiO)_2CO_3$ microspheres.

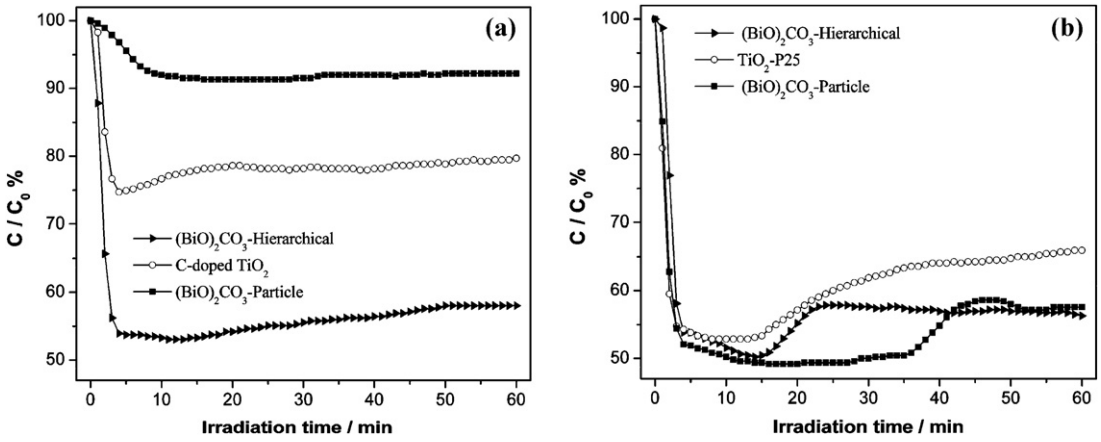

Fig. 7. Photocatalytic activities of hierarchical $(BiO)_2CO_3$ microspheres, $(BiO)_2CO_3$ particles, C-doped TiO_2 and TiO_2-P25 under visible (a) and UV (b) light irradiation for NO removal in indoor air.

60 min irradiation, the photodegradation rate of NO over $(BiO)_2CO_3$ particles is merely 8.0%. For C-doped TiO_2, the NO removal rate reaches at 20.5% due to its well known good visible light activity. Interestingly, the as-prepared hierarchical $(BiO)_2CO_3$ microspheres exhibits higher photocatalytic activity (42.0% of NO removal rates) under visible light irradiation than that of C-doped TiO_2, although the BET surface area and the pore volume are much smaller than that of C-doped TiO_2 (Table 1). The higher photocatalytic activity of hierarchical $(BiO)_2CO_3$ microspheres could mainly be attributed to the hierarchical structure. The hierarchical structure was favorable for the diffusion of reaction intermediates and the efficient utilization of photo-energy, thus enhancing the photocatalytic activity [2,33,48,58].

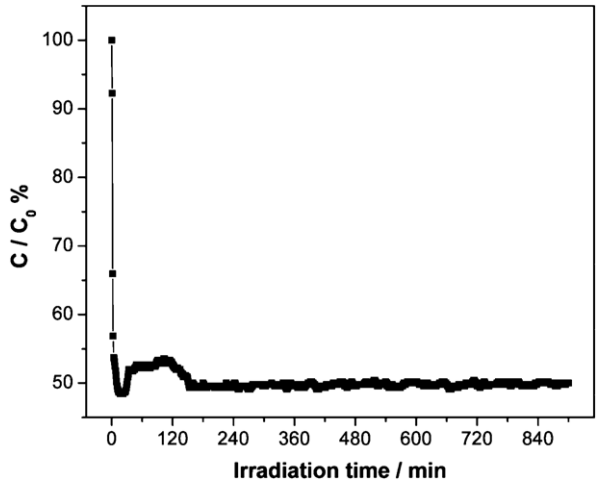

Fig. 8. Long term photocatalytic activity of hierarchical $(BiO)_2CO_3$ microspheres.

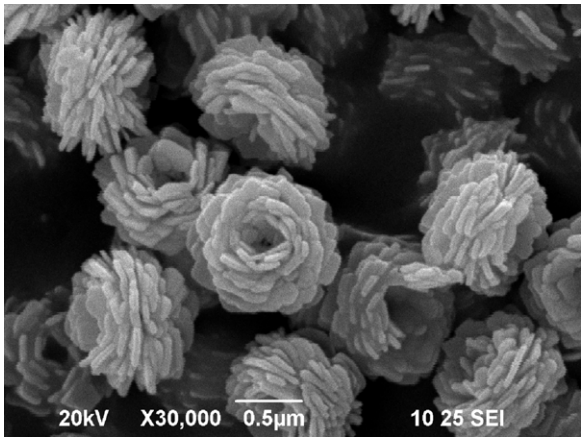

Fig. 9. SEM image of hierarchical $(BiO)_2CO_3$ microspheres after long time irradiation.

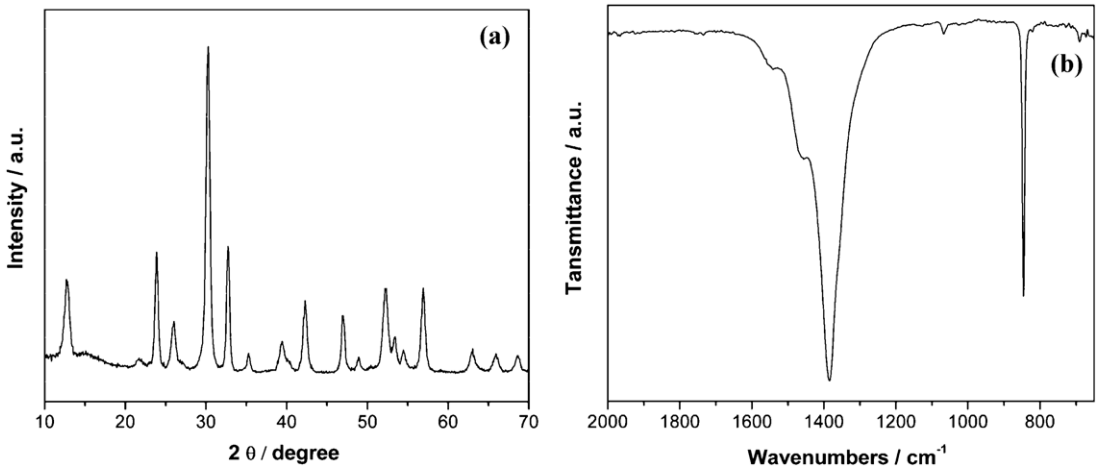

Fig. 10. XRD pattern (a) and FTIR spectra (b) of hierarchical $(BiO)_2CO_3$ microspheres after long time irradiation.

There are two band gaps of 2.0 and 3.25 eV for the hierarchical $(BiO)_2CO_3$ microspheres. The excellent visible light photocatalytic activity corresponds to the suitable band gap energy of 2.0 eV. For the band gap of 3.25 eV, we test the photocatalytic activity under UV irradiation, as shown in Fig. 7b. P25 is a famous excellent UV light photocatalyst, which naturally shows decent activity (removal rate of 35.1%) under UV irradiation. Interestingly, the hierarchical $(BiO)_2CO_3$ microspheres exhibit even higher activity (removal rate of 43.5%) than that of P25 and $(BiO)_2CO_3$ particles (removal rate of 42.5%) and under UV irradiation. Although the BET surface areas of hierarchical $(BiO)_2CO_3$ microspheres is much smaller than that of P25, the pore volume is larger than that of P25 (see Table 1). Large pore volume is favorable for the adsorption of reactant and diffusion of reaction intermediates. Compared to $(BiO)_2CO_3$ particles, the hierarchical structure of $(BiO)_2CO_3$ microspheres contributed to the enhanced photocatalytic activity under UV irradiation [2,33,48,58].

3.7.2. Long term photocatalytic activity and photochemical stability

The stability of a photocatalyst under irradiation should be considered for its practical application [57]. It would be most desirable if the photocatalyst can maintain durable activity so that the catalyst can be used for a long time. Some photocatalysts often suffer from instability for air purification applications, because the intermediates generated during photocatalytic reaction can accumulate on the catalyst surface, which possibly deactivates the photocatalyst. Fig. 8 shows long term photocatalytic activity of hierarchical $(BiO)_2CO_3$ microspheres under simulated solar irradiation. It can be seen that the photocatalytic activity is very stable during the photocatalytic oxidation of NO without deactivation. SEM image of hierarchical $(BiO)_2CO_3$ microspheres after long time irradiation is shown in Fig. 9. The morphology is almost the same as the SEM in Fig. 3b, indicating the microstructure doesn't change after long irradiation.

The stability of the hierarchical $(BiO)_2CO_3$ microspheres is further confirmed by XRD pattern and FI-TR spectra of hierarchical $(BiO)_2CO_3$ microspheres after long time irradiation, as shown in Fig. 10. The XRD pattern in Fig. 10a of the used $(BiO)_2CO_3$ microspheres shows that the crystal structure was not changed after the photocatalytic reaction, suggesting its phase stability. It can be seen from Fig. 10b that the reaction intermediates and products during photocatalytic oxidation of NO (such as HNO_2 and HNO_3) cannot be observed except for the vibration mode of $(BiO)_2CO_3$, which suggest that the reaction intermediates and products could diffuse rapidly due to the hierarchical structure. This is another reason for the excellent photochemical stability of hierarchical $(BiO)_2CO_3$ microspheres. As the solar light consists of both UV and visible light, our hierarchical $(BiO)_2CO_3$ hollow microspheres could fully use the solar light to remove the environmental pollutants by photocatalysis.

Table 1
BET specific surface areas and pore parameters of as-prepared $(BiO)_2CO_3$, C-doped TiO_2 and P25.

Samples	S_{BET} (m^2/g)	Total volume (cm^3/g)	Peak diameter (nm)
$(BiO)_2CO_3$	16.5	0.114	3.6/23.0
C-doped TiO_2	122.5	0.248	3.5
P25	51.2	0.090	22.0

4. Conclusions

Uniform monodisperse hierarchical $(BiO)_2CO_3$ hollow microspheres were successfully fabricated by one-pot template-free method. The hierarchical $(BiO)_2CO_3$ superstructure was constructed by the self-assembly of single-crystalline nanosheets. The aggregation of nanosheets produced three dimensional hierarchical structures containing mesopores and macropores, which was favorable for efficient transport of reaction molecules and harvesting of photo-energy. The results confirmed the existence of two-band-gap structure of 3.25 and 2.0 eV for $(BiO)_2CO_3$. In situ doped nitrogen contributed to the band gap of 2.0 eV by formation of mid-gap energy through substitution for oxygen atom in lattice. Owing to the attractive hierarchical hollow microstructure, and the high charge separation efficiency and special two-band-gap structure, the as-prepared $(BiO)_2CO_3$ microspheres not only exhibited excellent photocatalytic activity under both visible and UV light irradiation but also excellent photochemical stability during long term photocatalytic reaction for removal of NO in indoor air. The monodisperse hollow microspheres with hierarchical structure prepared by a facile method should find wide applications in environmental pollution control, solar energy conversion, catalysis and other related areas.

Acknowledgements

This research is financially supported by the National Natural Science Foundation of China (51108487), National High Technology Research and Development Program (863 Program) of China (2010AA064905), Research Grants of Chongqing Technology and Business University (2010-56-13), the Research Grants Council of Hong Kong (PolyU 5204/07E and PolyU 5175/09E), the Hong Kong

Polytechnic University (GU712, GYX75 and GYX0L), the Program for Chongqing Innovative Research Team Development in University (KJTD201020) and the Chongqing Key Natural Science Foundation (CSTC, 2008BA4012).

Appendix A. Supplementary data

Supplementary data associated with this article can be found, in the online version, at doi:10.1016/j.jhazmat.2011.08.050.

References

[1] T. Douglas, A bright bio-inspired future, Science 299 (2003) 1192–1193.
[2] H.X. Li, Z.F. Bian, J. Zhu, D.Q. Zhang, G.S. Li, Y.N. Huo, H. Li, Y.F. Lu, Mesoporous titania spheres with tunable chamber stucture and enhanced photocatalytic activity, J. Am. Chem. Soc. 129 (2007) 8406–8407.
[3] Y.F. Lu, H.Y. Fan, A. Stump, T.L. Ward, T. Rieker, J.C. Brinker, Aerosol-assisted self-assembly of mesostructured spherical nanoparticles, Nature 398 (1999) 223–226.
[4] J.N. Cha, G.D. Stucky, D.E. Morse, T.J. Deming, Biomimetic synthesis of ordered silica structures mediated by block copolypeptides, Nature 403 (2000) 289–292.
[5] X.W. Lou, L.A. Archer, Z.C. Yang, Hollow micro-/nanostructures: synthesis and applications, Adv. Mater. 20 (2008) 3987–4019.
[6] Y. Zhao, L. Jiang, Hollow micro/nanomaterials with multilevel interior structures, Adv. Mater. 21 (2009) 3621–3638.
[7] L.P. Zhu, H.M. Xiao, W.D. Zhang, G. Yang, S.Y. Fu, One-Pot template-free synthesis of monodisperse and single-crystal magnetite hollow spheres by a simple solvothermal route, Cryst. Growth Des. 8 (2008) 957–963.
[8] Y.H. Zheng, Y. Cheng, Y.S. Wang, L.H. Zhou, F. Bao, C. Jia, Metastable γ-MnS hierarchical architectures: synthesis, characterization, and growth mechanism, J. Phys. Chem. B 110 (2006) 8284–8288.
[9] J.G. Yu, H.G. Yu, H.T. Guo, M. Li, S. Mann, Spontaneous formation of a tungsten trioxide sphere-in-shell superstructure by chemically induced self-transformation, Small 4 (2008) 87–91.
[10] L.S. Zhang, W.Z. Wang, L. Zhou, H.L. Xu, Bi_2WO_6 nano- and microstructures: shape control and associated visible-light-driven photocatalytic activities, Small 3 (2007) 1618–1625.
[11] M. Yang, J. Ma, C.L. Zhang, Z.Z. Yang, Y.F. Lu, General synthetic route toward functional hollow spheres with double-shelled structures, Angew. Chem. Int. Ed. 44 (2005) 6727–6729.
[12] J.G. Yu, X.X. Yu, Hydrothermal synthesis and photocatalytic activity of zinc oxide hollow spheres, Environ. Sci. Technol. 42 (2008) 4902–4907.
[13] S.W. Kim, M. Kim, W.Y. Lee, T. Hyeon, Fabrication of hollow palladium spheres and their successful application to the recyclable heterogeneous catalyst for Suzuki coupling reactions, J. Am. Chem. Soc. 124 (2002) 7642–7643.
[14] J.H. Gao, B. Zhang, X.X. Zhang, B. Xu, Magnetic dipolar interaction induced self-assembly affords wires of cobalt selenide hollow nanoscrystals, Angew. Chem. Int. Ed. 45 (2006) 1220–1223.
[15] A.D. Dinsmore, M.F. Hsu, M.G. Nikolaides, M. Marquez, A.R. Bausch, D.A. Weitz, Colloidosomes: selectively permeable capsules composed of colloidal particles, Science 298 (2002) 1006–1009.
[16] Y.S. Li, J.L. Shi, Z.L. Hua, H.R. Chen, M.L. Ruan, D.S. Yan, Hollow spheres of mesoporous aluminosilicate with a three-dimensional pore network and extraordinarily high hydrothermal stability, Nano Lett. 3 (2003) 609–612.
[17] H.G. Yang, H.C. Zeng, Creation of intestine-like interior space for metal-oxide nanostructures with a quasi-reverse emulsion, Angew. Chem. Int. Ed. 43 (2004) 5206–5209.
[18] D.H.M. Buchold, C. Feldmann, Nanoscale γ-AlO(OH) hollow spheres: synthesis and container-type functionality, Nano Lett. 7 (2007) 3489–3492.
[19] J. Zhou, W. Wu, D. Caruntu, M.H. Yu, A. Martin, J.F. Chen, C.J. O'Connor, W.L. Zhou, Synthesis of porous magnetic hollow silica nanospheres for nanomedicine application, J. Phys. Chem. C 111 (2007) 17473–17477.
[20] H.C. Zeng, Curr, Ostwald ripening: a synthetic approach for hollow nanomaterials, Curr. Nanosci. 3 (2007) 177–181.
[21] H.J. Fan, U. Gösele, M. Zacharias, Formation of nanotubes and hollow nanoparticles based on Kirkendall and diffusion processes: a review, Small 3 (2007) 1660–1671.
[22] J. Zhang, F. Huang, Z. Lin, Progress of nanocrystalline growth kinetics based on oriented attachment, Nanoscale 2 (2010) 18–34.
[23] X.B. Chen, S.H. Shen, L.J. Guo, S.S. Mao, Semiconductor-based photocatalytic hydrogen generation, Chem. Rev. 110 (2010) 6503–6570.
[24] G. Zhang, W. Choi, S.H. Kim, S.B. Hong, Selective photocatalytic degradation of aquatic pollutants by titania encapsulated into FAU-type zeolites, J. Hazard. Mater. 188 (2011) 198–205.
[25] F. Dong, W.R. Zhao, Z.B. Wu, Characterization and photocatalytic activities of C N and S co-doped TiO_2 with 1D nanostructure prepared by nano-confinement effect, Nanotechnology 19 (2008) 365607.
[26] C.C. Chen, W.H. Ma, J.C. Zhao, Semiconductor-mediated photodegradation of pollutants under visible-light irradiation, Chem. Soc. Rev. 39 (2010) 4206–4219.
[27] S. Rehman, R. Ullah, A.M. Butt, N.D. Gohar, Strategies of making TiO_2 and ZnO visible light active, J. Hazard. Mater. 170 (2009) 560–569.
[28] P.L. Zhang, S. Yin, T. Sato, The influence of synthesis method on the properties of iron contained N doped TiO_2 photocatalysts, Appl. Catal. B 103 (2011) 462–469.
[29] F. Dong, H.Q. Wang, S. Guo, Z.B. Wu, S.C. Lee, Enhanced visible light photocatalytic activity of novel Pt/C-doped $TiO_2/PtCl_4$ three-component nanojunction system for degradation of toluene in air, J. Hazard. Mater. 187 (2011) 509–516.
[30] X.L. Hu, G.S. Li, J.C. Yu, Design, Fabrication, and modification of nanostructured semiconductor materials for environmental and energy applications, Langmuir 26 (2010) 3031–3039.
[31] J. Kim, C.W. Lee, W. Choi, Platinized WO_3 as an environmental photocatalyst that generates OH radicals under visible light, Environ. Sci. Technol. 44 (2010) 6849–6854.
[32] J.H. Mo, Y.P. Zhang, Q.J. Xu, Y.F. Zhu, J.J. Lamson, R.Y. Zhao, Determination and risk assessment of by-products resulting from photocatalytic oxidation of toluene, Appl. Catal. B 89 (2009) 570–576.
[33] J.G. Yu, Y.R. Su, B. Cheng, Template-free fabrication and enhanced photocatalytic activity of hierarchically macro/mesoporous titania, Adv. Funct. Mater. 17 (2007) 1984–1990.
[34] Y.J. Wang, R. Shi, J. Lin, Y.F. Zhu, Significant photocatalytic enhancement in methylene blue degradation of TiO_2 photocatalysts via graphene-like carbon in situ hybridization, Appl. Catal. B 100 (2010) 179–183.
[35] X.X. Yu, J.G. Yu, B. Cheng, B.B. Huang, One-pot template-free synthesis of monodisperse zinc sulfide hollow spheres and their photocatalytic properties, Chem. Eur. J. 15 (2009) 6731–6739.
[36] D. Chen, J.H. Ye, Hierarchical WO_3 hollow shells: dendrite sphere, dumbbell, and their photocatalytic properties, Adv. Funct. Mater. 18 (2008) 1922–1928.
[37] W.Z. Yin, W.Z. Wang, M. Shang, L. Zhou, S.M. Sun, L. Wang, $BiVO_4$ hollow nanospheres: anchoring synthesis, growth mechanism, and their application in photocatalysis, Eur. J. Inorg. Chem. 437 (2009) 9–4384.
[38] L.S. Zhang, W.Z. Wang, Z.G. Chen, L. Zhou, H.L. Xu, W. Zhu, Fabrication of flower-like Bi_2WO_6 superstructures as high performance visible-light driven photocatalysts, J. Mater. Chem. 17 (2007) 2526–2532.
[39] I.S. Cho, D.W. Kim, S.W. Lee, C.H. Kwak, S.T. Bae, J.H. Noh, S.H. Yoon, H.S. Jung, D.W. Kim, K.S. Hon, Synthesis of Cu_2PO_4OH hierarchical superstructures with photocatalytic activity in visible light, Adv. Funct. Mater. 18 (2008) 2154–2162.
[40] P. Aylor, S. Sundek, V. Lopata, Structure, spectra, and stability of solid bismuth carbonates, Can. J. Chem. 62 (1984) 2863–2873.
[41] R. Chen, M.H. So, J. Yang, F. Deng, C.M. Che, H.Z. Sun, Fabrication of bismuth subcarbonate nanotube arrays from bismuth citrate, Chem. Commun. 226 (2006) 5–2267.
[42] Y. Zheng, F. Duan, M.Q. Chen, Y. Xie, Synthetic $Bi_2O_2CO_3$ nanostructures: novel photocatalyst with controlled special surface exposed, J. Mol. Catal. A: Chem. 317 (2010) 34–40.
[43] H.F. Cheng, B.B. Huang, K.S. Yang, Z.Y. Wang, X.Y. Qin, X.Y. Zhang, Y. Dai, Facile template-free synthesis of $Bi_2O_2CO_3$ hierarchical microflowers and their associated photocatalytic activity, ChemPhysChem 11 (2010) 2167–2173.
[44] C.Z. Wu, Y. Xie, Controlling phase and morphology of inorganic nanostructures originated from the internal crystal structure, Chem. Commun. 594 (2009) 3–5957.
[45] G.E. Tobon-Zapata, S.B. Etcheverry, E.J. Baran, Vibrational spectrum of bismuth subcarbonate, J. Mater. Sci. Lett. 16 (1997) 656–657.
[46] K.S.W. Sing, D.H. Everett, R.A.W. Haul, L. Moscou, R.A. Pierotti, J. Rouquerol, T. Siemieniewska, Reporting physisorption data for gas/solid systems, Pure Appl. Chem. 57 (1985) 603–619.
[47] X.C. Wang, J.C. Yu, C.M. Ho, Y.D. Hou, X.Z. Fu, Photocatalytic activity of a hierarchically macro/mesoporous titania, Langmuir 21 (2005) 2552–2559.
[48] F. Dong, W.R. Zhao, Z.B. Wu, S. Guo, Band structure and visible light photocatalytic activity of multi-type nitrogen doped TiO_2 nanoparticles prepared by thermal decomposition, J. Hazard. Mater. 162 (2008), 763-760.
[49] S. Shamaila, A.K.L. Sajjad, F. Chen, J.L. Zhang, Study on highly visible light active Bi_2O_3 loaded ordered mesoporous titania, Appl. Catal. B 94 (2010) 272–280.
[50] X.B. Chen, C. Burda, Photoelectron spectroscopic investigation of nitrogen-doped titania nanoparticles, J. Phys. Chem. B 108 (2004) 15446–15449.
[51] Y. Cong, J.L. Zhang, F. Chen, M. Anpo, D.N. He, Preparation, photocatalytic activity, and mechanism of nano-TiO_2 co-doped with nitrogen and iron (III), J. Phys. Chem. C 111 (2007) 10618–10623.
[52] Z.B. Wu, F. Dong, W.R. Zhao, S. Guo, Visible light induced electron transfer process over nitrogen doped TiO_2 nanocrystals prepared by oxidation of titanium nitride, J. Hazard. Mater. 157 (2008) 57–63.
[53] X.B. Chen, C. Burda, The Electronic origin of the visible-light absorption properties of C-, N- and S-doped TiO_2 nanomaterials, J. Am. Chem. Soc. 130 (2008) 5018–5019.
[54] X.B. Chen, P.A. Glans, X. Qiu, S. Dayal, W.D. Jennings, K.E. Smith, C. Burda, J. Guo, X-ray spectroscopic study of the electronic structure of visible-light responsive N-, C- and S-doped TiO_2, J. Electron. Spectrosc. 162 (2008) 75–81.
[55] S.U.M. Khan, M. Al-Shahry, W.B. Ingler Jr., Efficient photochemical water splitting by a chemically modified *n*-TiO_2, Science 297 (2002) 2243–2245.
[56] C.S. Pan, Y.F. Zhu, New type of $BiPO_4$ oxy-acid salt photocatalyst with high photocatalytic activity on degradation of dye, Environ. Sci. Technol. 44 (2010) 5570–5574.
[57] Z.H. Ai, W.K. Ho, S.C. Lee, L.Z. Zhang, Efficient photocatalytic removal of NO in indoor air with hierarchical bismuth oxybromide nanoplate microspheres under visible light, Environ. Sci. Technol. 43 (2009) 4143–4150.
[58] G.S. Li, D.Q. Zhang, J.C. Yu, M.K.H. Leung, An efficient bismuth tungstate visible-light-driven photocatalyst for breaking down nitric oxide, Environ. Sci. Technol. 44 (2010) 4276–4281.